Pergamon

Int. J. Multiphase Flow Vol. 24, No. 2, pp. 165–188, 1998

Printed in Great Britain
PII: S0301-9322(97)00055-4
0301-9322/98 $19.00 + 0.00

HEAT TRANSFER IN INTERMITTENT AIR–WATER FLOWS—PART I

HORIZONTAL TUBE

G. HETSRONI, B. G. HU, J. H. YI, A. MOSYAK, L. P. YARIN and G. ZISKIND
Faculty of Mechanical Engineering, Technion—Israel Institute of Technology, Haifa 32000, Israel

(Received 6 January 1997; in revised form 28 July 1997)

Abstract—This paper presents a study on the heat transfer in intermittent air–water flows in a horizontal tube. The experimental technique is based on infrared thermography of an electrically heated wall of the tube, providing both visualization of the temperature field and measurements of the local wall temperature. Measurements of bubble size and frequency are correlated to the measurements of the local wall temperature fluctuations and heat transfer coefficient. The water and air Froude numbers varied from 0.9 to 2.0 and from 0.03 to 0.43, respectively. On the upper part of the tube, the effect of the gas Froude number is as follows. In the range $Fr_G < 0.13$ heat transfer decreases with increasing Fr_G, while in the range $0.13 < Fr_G < 0.43$ the heat transfer increases when Fr_G increases. On the lower part of the tube the heat transfer coefficient does not depend on the gas Froude number. © 1998 Elsevier Science Ltd. All rights reserved

Key Words: horizontal tube, air–water flow, heat transfer

1. INTRODUCTION

The effect of bubbles on flow pattern and transport properties is of great importance in many modern industrial applications where heat or mass transfer is involved. Examples of these applications are absorption of gases, fermentation, sewage purification process, direct contact heat exchangers, etc. In spite of its importance, there exists a limited ability to predict the heat transfer in these systems, and there is a lack of understanding on how bubble size distribution and an interaction of bubbles with the flow affect the heat transfer, especially at low gas velocities.

Our study deals with heat transfer in horizontal, inclined, and vertical tubes. In addition to the common features, each case has its own properties, sometimes very different from those encountered in the other cases. For this reason, we present in this paper the results concerning a horizontal tube only. These results will serve as a reference basis for the study on inclined tubes, presented in Part II, and for the future study on vertical tubes. A distinctive feature of these studies is that we obtain and analyse a thermal pattern on the heated wall, which makes it possible to establish the connection between the flow parameters and heat transfer. The experimental technique is based on infrared thermography of an electrically heated wall of the tube, providing both visualization of the temperature field and measurements of the local wall temperature. This technique has been successfully used by Hetsroni and Rozenblit (1994).

A variety of complex intermittent flows can exist in horizontal tubes. This complexity results from the intermittent nature of the flow and the large velocity gaps between the various slug regions. The phenomena associated with the moving slug front are of a high degree of complexity due to the moving free interface (Moalem Maron *et al.* 1991). The slug flow regime is well investigated for a horizontal flow (Dukler and Hubbard 1975; Kokal and Stanislav 1989; Lin and Hanratty 1986; Spedding and Spence 1993; Taitel and Dukler 1976). Andritsos and Hanratty (1987) investigated the effect of the interfacial instabilities in a horizontal flow that led them to the determination of different types of waves. Foukano and Ousaka (1989) proposed a model based on the pumping action of waves which propagate along the pipe walls. Small waves initialize droplet atomization and lead to droplet deposition on the pipe walls at higher

gas and lower liquid superficial velocities. Several investigations have been carried out on droplet atomization, entrainment and deposition (e.g. Paras and Karabellas 1991; Wallis 1968; Whalley and Hewitt 1978). Woods and Hanratty (1996) studied the initiation of slug flow regime at high gas velocities.

Johnson and Abou-Sabe (1952) and Fried (1954) used several thermocouples on the tube wall and reported variations in wall temperature. The data on the heat transfer in air–water flow were correlated by Hughmark (1965). Shoham *et al.* (1982) observed fluctuations in the wall temperature and heat transfer rate in time and around the pipe circumference. Measurements for a 0.171 m diameter pipe were reported by Mehta (1984). Kago *et al.* (1986) observed differences in the wall temperature between the top and the bottom and showed that in the range of superficial gas velocity $U_{GS} = 0.2$–1.0 m/s the average heat transfer coefficient was nearly independent of the gas velocity. Deshpande *et al.* (1991) studied the circumferential variation of heat transfer rates during a plug–slug flow. The dimensionless correlations based on the superficial liquid and gas velocity were given for the pipe top and bottom. The analysis reported by Sun *et al.* (1994) shows that for a calculation of the heat transfer coefficient for nucleate boiling, one needs to know the heat transfer coefficient for the forced convection in a single phase.

In the studies of heat transfer in turbulent air–water flows, the two-phase flow is usually treated as a two-phase mixture. In the present study the liquid and gas phases are intermittent and different entities. We address such questions as the local fluctuation of wall temperature, difference between temperatures of the upper and lower parts of the tube wall, the heat transfer coefficient and its dependence on the peripheral position in an intermittent flow.

The experiments also resulted in detailed knowledge of bubble size, frequency, and velocity, as depending on the flow rates of both phases. These results are correlated to the measurements of the local wall temperature fluctuation and the heat transfer coefficient distribution on the upper part of the tube. For the lower part of the tube, we provide information on the distribution of the heat transfer coefficient and thermal streak pattern. The heat transfer coefficients are determined for clearly identified flow patterns.

2. DESCRIPTION OF THE EXPERIMENTS

2.1. *Experimental apparatus*

A schematic diagram of the experimental facility is presented in figure 1. The 6850 mm long horizontal smooth test section consists of four parts: the development section, the section of

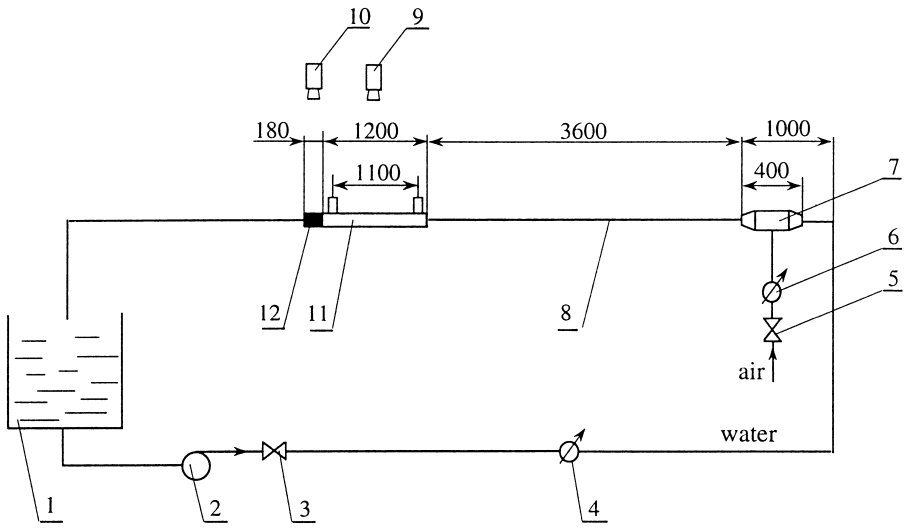

Figure 1. Experimental facility: 1, tank; 2, pump; 3, flow regulator; 4, water flowmeter; 5, air regulator; 6, air flowmeter; 7, mixing section; 8, development section; 9, video camera; 10, IR camera; 11, pressure measurement section; 12, heated test section.

flow visualization and pressure drop measurements, the heated test section and the outlet section. The 3600 mm long development section and the 1870 mm long outlet section are made of 49.2 mm inner diameter plastic tube. The glass section, for flow visualization and pressure drop measurements, was also of 49.2 mm inner diameter. The pressure drop in this section was measured across 1100 mm length by means of two external manifolds, which were connected to pressure transducers. The upstream tap was 74 tube diameters from the entrance to the visualization section, while the downstream tap was 39 diameters from the exit. A 400 mm long, 220 mm inner diameter mixing chamber was used to deliver air to the development section. Air entered through a 12.2 mm inner diameter pipe at the bottom of the mixing chamber and passed through a porous layer with a mean pore diameter of 0.12 mm. As a result, bubbles were formed and then mixed with the water stream. The pipe was carefully levelled because of the sensitivity of flow regime transitions to the pipe inclination. Water, at a constant temperature, was circulated from the tank through the loop by means of a pump. The bubbles were removed at the upper part of the tank.

After passing through the pressure measurement section, the air–water mixture passed through the heated section for visualization of the thermal pattern on the wall, and for temperature measurements. This section, shown in figure 2(a), was constructed of a 50 μm thick

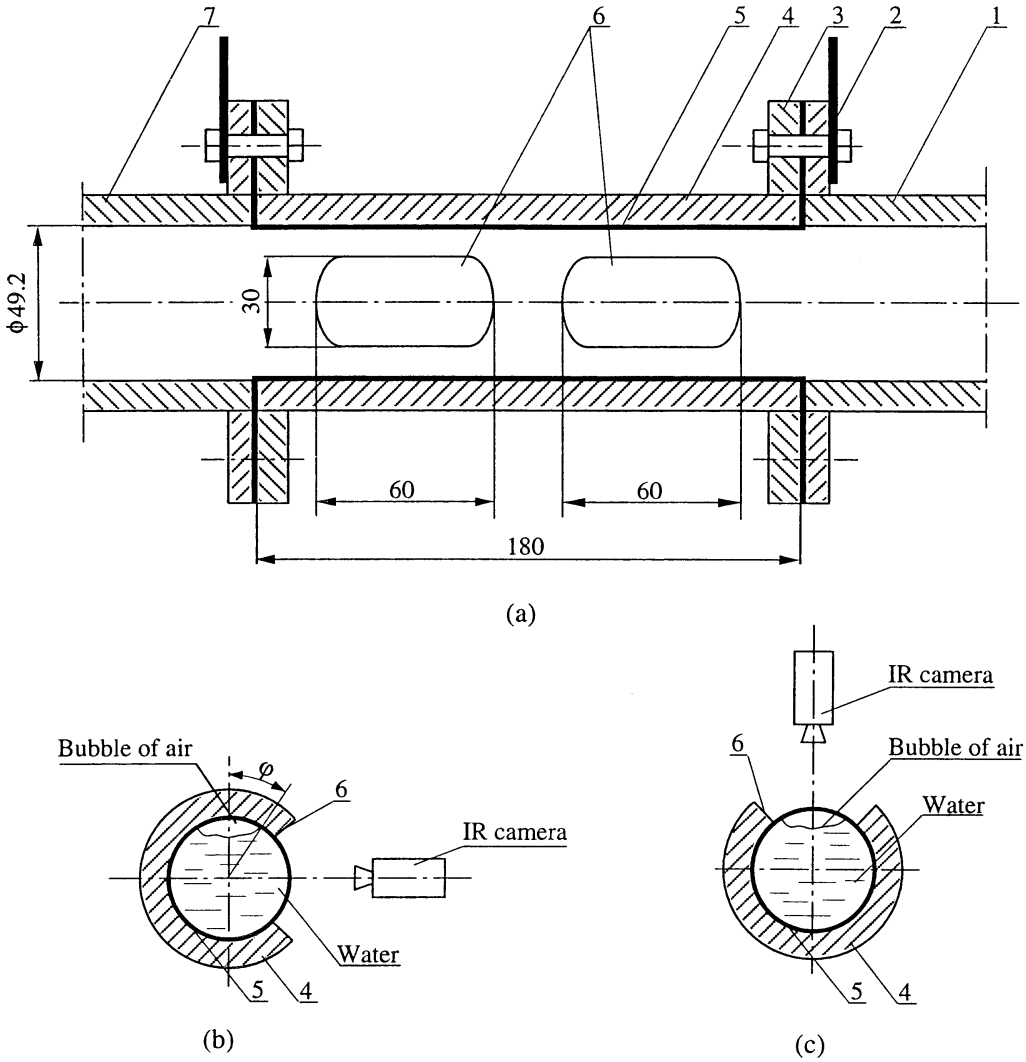

Figure 2. The test section and methods of wall temperature measurement: (a) the test section; (b) temperature measurements on the lower part of the tube; (c) temperature measurements on the upper part of the tube: 1, development section; 2, electrical contact; 3, aluminum flanges; 4, plastic tube; 5, constantan foil; 6, windows; 7, outlet section.

constantan foil on the inner wall of the plastic tube. Heating was done by applying DC current, from a controlled power supply. The heated section was 180 mm long with two windows, each of $30 \times 60\ \text{mm}^2$. Heating of the wall began about 97 diameters downstream of the entrance to the development section and heat transfer measurements were made at about two diameters downstream from the entrance of the heating section. The heating section can be rotated around the horizontal axis to put the heating surface in a desired orientation. Figure 2(b,c) shows the methods of wall temperature measurements.

2.2. *Measurement techniques*

The motion of bubbles in the pipe was studied by analysing video images. The method is based on the detection of the edges of bubbles in a sequence of video frames. This method allows us to measure the length, size and velocity of elongated bubbles. The bubble motion of intermittent flow was recorded consecutively by a 3CCD video camera. The illumination was provided by a set of 500 W halogen lamps, mounted on a frame at the opposite side of the test section. Pictures were taken with a black background, so that the bubbles had a white outline. The camera provided the video signal which consists of two fields, represented by the odd and even rows of the image, respectively. For a PAL video system, the time interval between the two fields is 1/50 s. Each video frame thus produces two bubble images at the effective sampling frequency of 50 Hz. Each run a sequence of at least 120 s was recorded. In the playback mode, typical flow patterns were frozen on the TV monitor and analysed frame by frame to calculate the average bubble length, height and frequency for each set of the data.

At low gas velocities, the flow consists of elongated gas bubbles which move along the upper part of the pipe. Neglecting aeration, in developing necessary conditions for the existence of slugging, may introduce errors in the analysis of the slugging front and tail behaviour. However, for the case of moderate aeration, this simplification may not be too serious (Ruder *et al*. 1989).

The Thermal Imaging Radiometer, was used in the investigation of thermal patterns. It has a typical horizontal and vertical resolution of 256 pixels per line. The radiometer allows us to obtain a qualitative thermal profile in the line mode, the average temperature in the area mode, and the temperature of a given point in the point mode. No calibration correction for a curved surface is required.

The experiments were carried out at a constant heat flux. We had to consider the frequency response of the system to changes in the heat transfer coefficient. For this purpose, we solved numerically the transient heat conduction problem. The magnitude of the heat transfer coefficient is proportional to $\cos(f\tau)$ where f is the frequency and τ is the time. It was shown by Hetsroni and Rozenblit (1994) that temperature distortions and phase shift in temperature fluctuations on the heated wall begin at $f = 15$–$20\ \text{s}^{-1}$. In the present study the highest frequency of bubbles did not exceed $7\ \text{s}^{-1}$.

A special computer program made it possible to store the information on the temperature fluctuations. Simultaneously, the thermal pattern was saved on a video tape. The video was then used, in playback mode, to analyse the data. The measured values of the temperature, at a distance $x/D = 2$ from the entrance of the heated section, were used for the heat transfer coefficient calculations.

The surface temperature and the air–water mixture temperature were measured with an accuracy of $\pm 0.1^{\circ}\text{C}$. The water flow was controlled by a valve and measured by a standard orifice plate with an accuracy of $\pm 1\%$. The air flow was measured by means of a mass flowmeter with an accuracy of $\pm 1\%$. The pressure was measured by the pressure transducers with an accuracy of $\pm 1\%$. Electrical power was determined by means of a digital wattmeter with an accuracy of $\pm 0.5\%$.

2.3. *Experimental procedure*

2.3.1. *Single-phase tests.* A number of verification runs were undertaken prior to the data logging. A series of single-phase water flow tests was made to establish the validity of the system and testing technique. The pressure drop results agree with the accepted smooth pipe values (Blasius equation) with a standard deviation of $\pm 2\%$.

Preliminary calculations (Hetsroni and Rozenblit 1994) have shown that the difference between the temperature of the two sides of the thin constantan foil, i.e. inside wall temperature

and outside wall temperature, is less than 0.1°C. The axial heat conduction for the heated test section was calculated using measurements of wall temperature distribution in the x direction in the range of heat flux q = 3–20 kW/m^2. The heat transfer in the axial direction was less than 0.5% of that in the radial one. Heat balance for the variation of the outside ambient temperature has also been verified by a direct measurement. The estimated total heat losses were in the range of 1–2%, depending on the values of the heat flux.

The time-averaged heat transfer coefficient in clear water is defined as

$$\alpha = q/(\bar{T}_W - \bar{T}_f) \quad [1]$$

where q is the heat flux, $\bar{T}_W$is the time-averaged wall temperature, $\bar{T}_f$ is the time-averaged mean value of the water temperature at the entrance and the exit of the heated section.

The experimental Nusselt numbers, based on the diameter, in the thermal entry length of a tube are shown in figure 3. The experimental data were compared with results calculated by using the k–ε model (solid lines). These calculations were carried out for a fully developed velocity profile, but with a uniform fluid temperature at the point where the heat transfer begins. Thus, we consider a developing temperature profile, i.e. *thermal* entry length x. The experimental and calculated values agree within ±12%.

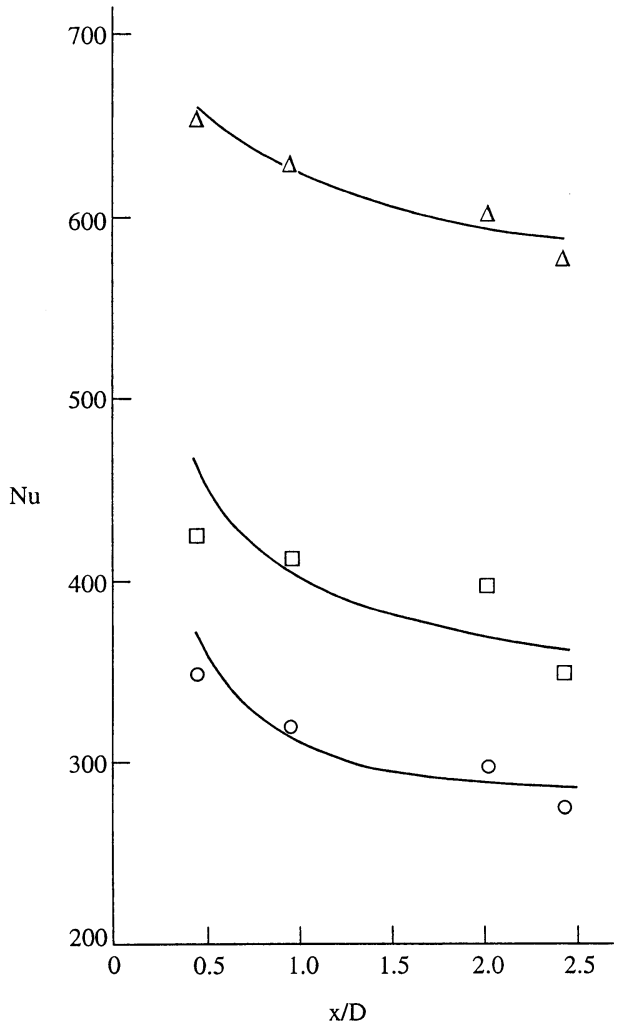

Figure 3. Nusselt numbers in the thermal entry length at various mean water velocities: ○, U = 0.62 m/s; □, U = 0.87 m/s; △, U = 1.4 m/s.

Table 1. Experimental conditions

Superficial liquid velocity U_{LS} (m/s)	Superficial gas velocity U_{GS} (m/s)	Heat flux $q \times 10^{-4}$ (W/m^2)
0.62	0.02	0.14
	0.05	0.07
	0.09	0.14
	0.22	0.38
	0.30	0.31
0.87	0.02	0.35
	0.05	0.24
	0.09	0.77
	0.22	0.80
	0.30	0.69
1.40	0.02	0.31
	0.05	1.13
	0.09	1.67
	0.22	1.90
	0.30	1.86

2.3.2. *Two-phase flow test procedure*. The water and air were mixed in a mixing chamber upstream of the test section. The method of mixing was selected from the previous investigations reported by Johnson and Abou-Sabe (1952). Two-phase tests were conducted at constant liquid flow rates, with various air flow rates. The experimental conditions are listed in table 1. The experiments were repeated to confirm their reproducibility. The distribution of bubble size becomes independent of the distance 83 diameters downstream of the mixing chamber. The heat transfer and flow parameters for each data run were measured under steady-state conditions, when the time-average values of the temperature and pressure were constant.

The time-averaged local heat transfer coefficient in air–water flow is defined as

$$\alpha_\theta = q/(\bar{T}_\theta - \bar{T}_f) \qquad [2]$$

where $\bar{T}_\theta$ is the time-averaged circumferential wall temperature, $\theta = 2\varphi/\pi$ is the dimensionless angle, φ is the angle from the top of the pipe.

We carried out measurements of the heat transfer coefficient at $\theta = 0$ at different locations along the tube. The distances from the entrance of the heating section to the measuring points were $x/D = 0.45$, 0.9, 2.0, and 2.4. For each set of flow conditions, the measurements were repeated at least three times. In the clear water flow, the measurements of the heat transfer coefficient α were carried out for the mean flow velocities of 0.62, 0.87 and 1.4 m/s. Then, the results were compared with the heat transfer coefficient $\alpha_{\theta=0}$ in the air–water flow. The experiments in the two-phase flow were carried out at the same water flow rates (i.e. superficial liquid velocities) for all superficial gas velocities given in table 1. The results for the superficial gas velocity $U_{GS} = 0.02$ and superficial liquid velocities are shown in figure 4(a); the results for $U_{GS} = 0.3$ and $U_{LS} = 0.62$, 0.87, and 1.4 m/s are shown in figure 4(b). It was found that the ratio of the heat transfer coefficient in air–water flow to the heat transfer coefficient in clear water, $\alpha_{\theta=0}/\alpha$, did not depend on x/D for $\theta = 0$.

3. ANALYTICAL CONSIDERATIONS

Before presenting the experimental results, it is of interest to discuss briefly the dimensionless parameters used in the analysis. An application of the Buckingham Pi theorem to the motion of air and water indicates that the following dimensionless groups can be found: $U_{LS}/\sqrt{gD}$, $U_{GS}/\sqrt{gD}$, $u_b/\sqrt{gD}$, L/D, H/D, ρ_G/ρ_L, μ_G/μ_L, $\sigma\rho_L D/\mu_L^2$, $\mathrm{Re}_L = U_{LS}D\rho_L/\mu_L$, $\mathrm{Re}_G = U_{GS}D\rho_G/\mu_G$, $A = fL/u_b$, α_θ/α, $\theta = 2\varphi/\pi$, where D is the pipe diameter, L is the bubble length, H is the bubble height, ρ_G, ρ_L and μ_G, μ_L are the density and viscosity of liquid and gas, respectively, U_{LS}, U_{GS} are the superficial liquid and gas velocity, respectively, f is the frequency of bubbles, u_b is the bubble velocity, σ is the surface tension, g is the acceleration due to gravity, α_θ is the heat transfer coefficient in air–water flow, α is the heat transfer coefficient in clear water (liquid single phase), φ is the angle shown in figure 2.

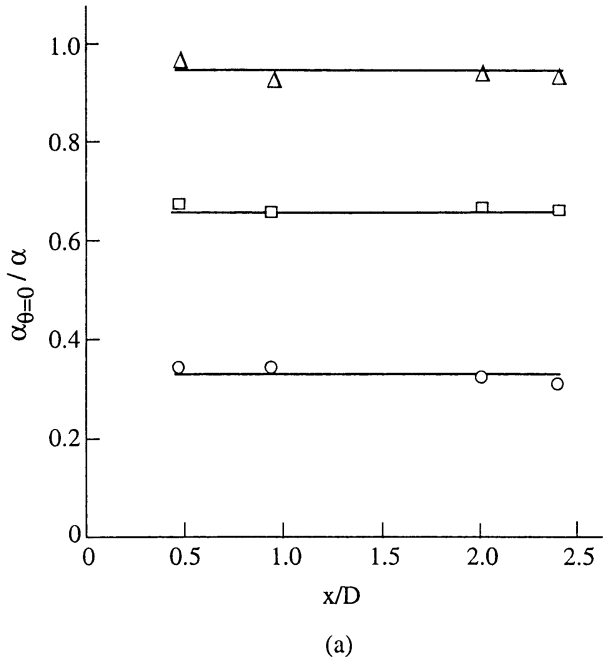

(a)

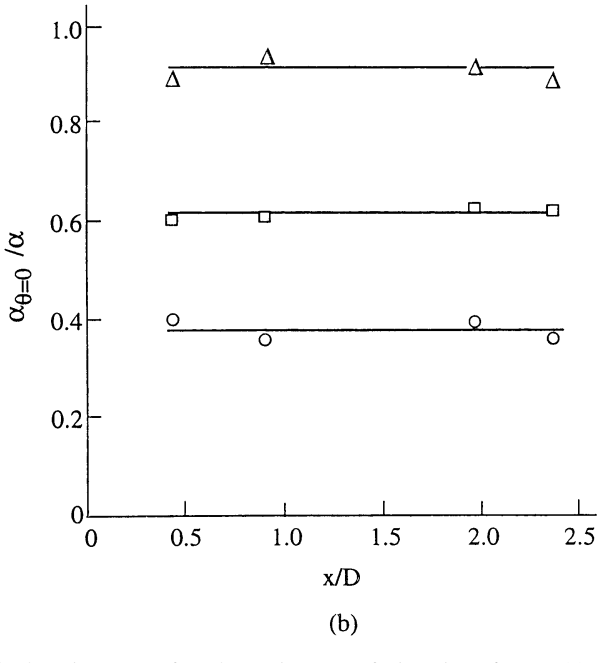

(b)

Figure 4. Dimensionless heat transfer along the top of the pipe, $\theta = 0$: (a) $U_{GS} = 0.02$ m/s; (b) $U_{GS} = 0.3$ m/s: ○, $U_{LS} = 0.62$ m/s; □, $U_{LS} = 0.87$ m/s; △, $U_{LS} = 1.40$ m/s.

Sets of alternate groups can, of course, be developed, but it is clear that in the analysis we do not use all the dimensionless groups shown above. This method is based on a reasonable guess of the 'important' dimensionless groups, whereas the influence of the others is considered less important.

We assume that the surface tension does not change, and that the value of $\bar{\alpha}$ does not depend on thermal properties of the fluids. For this reason, all the experiments were carried out when, in the heated section, the difference between the wall temperature and the mean temperature of the fluid did not exceed 10°C.

In the present study of an intermittent flow in horizontal tubes the following non-dimensional parameters were selected: L/D, H/D, $U_{LS}/\sqrt{gD}$, $U_{GS}/\sqrt{gD}$, $u_b/\sqrt{gD}$, $A = fL/u_b$, $\bar{\alpha} = \alpha_\theta/\alpha$, $\theta = 2\varphi/\pi$, $\mathrm{Re}_L = U_{LS}D\rho_L/\mu_L$.

When these groups are used to normalize the variables, we assume that the surface tension parameter, density and viscosity do not change in the experiment.

4. EXPERIMENTAL RESULTS

4.1. *Flow parameters*

4.1.1. *Flow pattern recognition*. A number of different methods have been proposed for the determination of flow patterns, ranging from visual observations to complicated methods for the analysis of pressure fluctuations (Barnea and Taitel 1986; Dukler and Hubbard 1975; Lin and Hanratty 1987; Spedding and Spence 1993). The flow regime in this work was identified by video recording and a visual observation.

Many investigators have studied the hydrodynamics of two-phase flow and attempted to define the boundaries between the various flow regimes. An early flow regime map, which was suggested by Mandhane *et al*. (1974), used the superficial phase velocities as mapping parameters. Taitel and Dukler (1976) developed an approach to derive the basic map from a fundamental level, while Barnea and Taitel (1986) and Jepson and Taylor (1993) have extended the general approach to include the effects of geometric and operational variables. The flow regime map suggested by Barnea and Taitel (1986) for the air–water mixture in a horizontal pipe is shown in figure 5. There are five primary flow regimes: dispersed bubble (DB), annular (A), stratified smooth (SS), stratified wavy (SW) and intermittent (I). In the present work, for each water flow rate a series of experiments with various air flow rates was carried out. The superficial velocities of the liquid phase U_{LS} and air phase U_{GS} were in the range 0.62–1.40 m/s and 0.02–0.30 m/s, respectively. All these experimental data are plotted in figure 5 and correspond to the intermittent flow regime.

4.1.2. *Bubble size*. The main characteristics of gas–liquid flow are intermittent and irregular. Each slug unit is composed of a liquid slug, containing dispersed bubbles, and an elongated bubble zone. Flow parameters, such as the length of the liquid slug and the length of the elongated bubbles, affect the heat transfer. Of particular importance are the bubble length, height and frequency, since it may be expected that the gas phase causes a non-uniform distribution of the local heat transfer coefficients.

Due to the unsteady character of the intermittent flow, these parameters are described in statistical terms, for each air–water flow regime, by detecting the bubble size distribution. The aver-

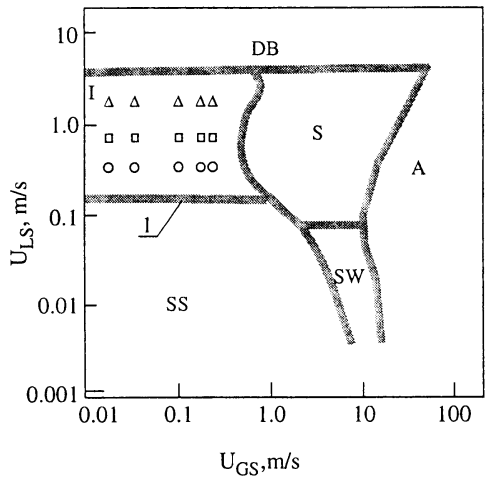

Figure 5. Flow-pattern map: A, annular flow; DB, dispersed bubble flow; I, intermittent flow; S, slug flow; SS, stratified smooth flow; SW, stratified wavy flow; 1, transition boundary: ○, $U_{LS} = 0.62$ m/s; □, $U_{LS} = 0.87$ m/s; △, $U_{LS} = 1.40$ m/s.

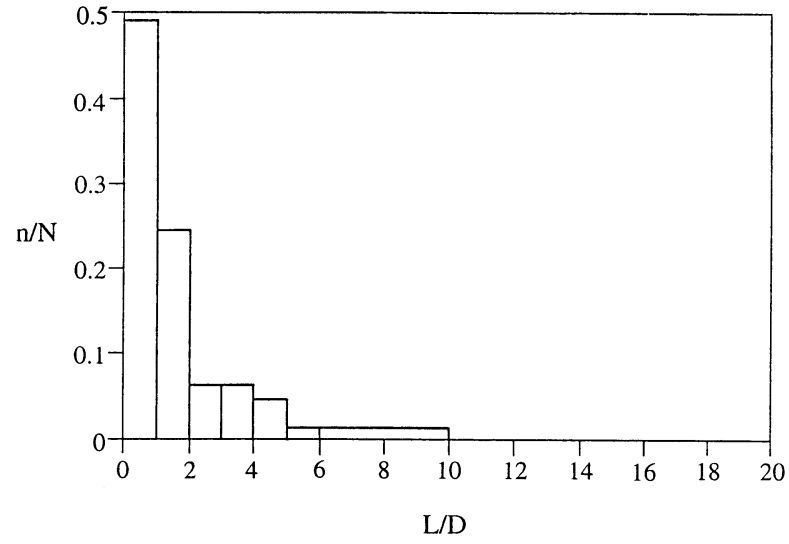

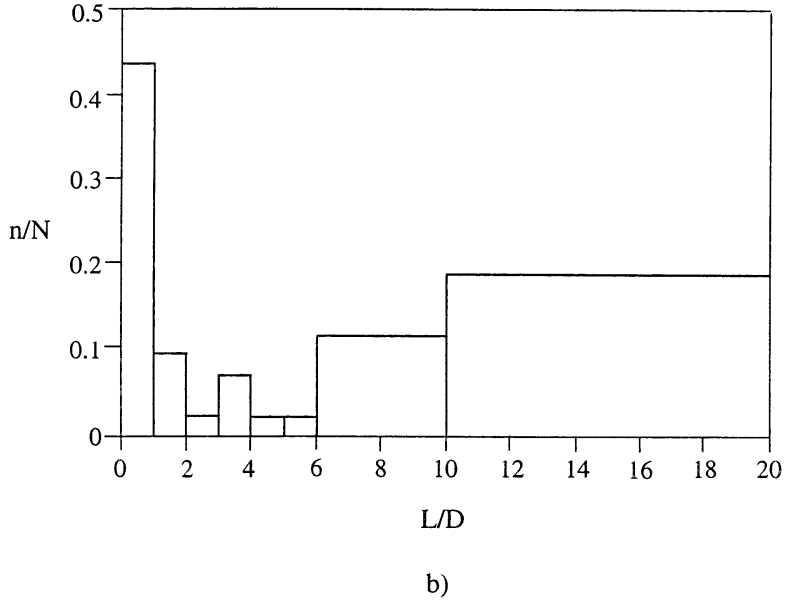

Figure 6. The typical histograms of the bubble length distribution at $U_{LS} = 1.40$ m/s: (a) $U_{GS} = 0.09$ m/s, (b) $U_{GS} = 0.3$ m/s.

age bubble length and height were calculated from the measured bubble size distribution for each experiment. 45 different flow conditions were checked. For each flow condition at least 300 individual data sets were recorded, and the average values of bubble length and height were calculated with standard deviation $\pm 12\%$. These calculations were performed for the fully developed state, when the bubble size distribution did not change in the flow direction.

Johnson and Abou-Sabe (1952) studied the heat transfer and pressure drop for a turbulent flow of air–water mixtures in a horizontal pipe, where water and air were mixed at 70 diameters upstream of the test section. The data presented by Hand and Spedding (1993) show that at $x/D = 92$ the horizontal gas–liquid flow is independent of x/D. The value of $x/D = 85$ used in the present work is close to their recommendations.

In figure 6(a,b) a typical histogram of the bubble length distribution at the location $x/D = 85$ is plotted. The plots show the relative number of bubbles of different length intervals, where the bubble length is normalized with pipe diameter. A rough criterion helping to distinguish between the elongated (Taylor) bubbles and the dispersed bubbles within the liquid slug is the characteristic value based on the pipe diameter. Bubbles with a chord length larger than the pipe diameter are considered as the elongated ones. Smaller bubbles are usually termed the dispersed ones. The superficial liquid velocity was $U_{LS} = 1.40$ m/s and the superficial gas velocities were $U_{GS} = 0.09$ m/s and $U_{GS} = 0.30$ m/s, respectively [figure 6(a,b)]. When U_{LS} is constant, an increase in U_{GS} causes an increase in bubble length. Figure 7(a) presents the average non-dimensional bubble length L/D vs. the gas Froude number for different superficial liquid velocities. The average bubble length is observed to be two to seven pipe diameters. An increase in the gas

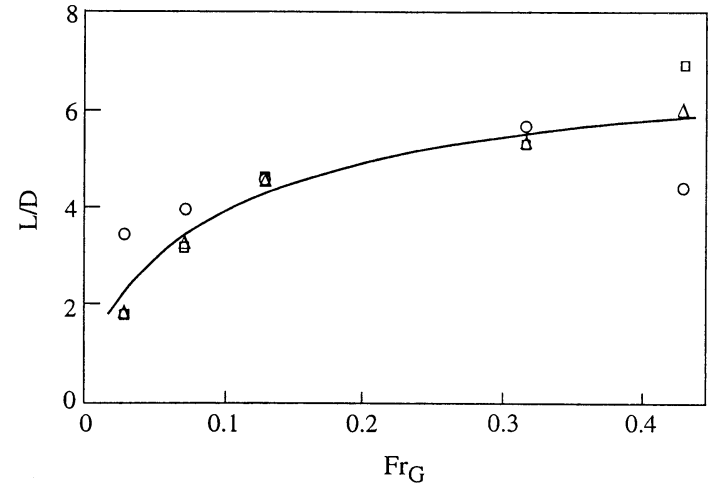

a)

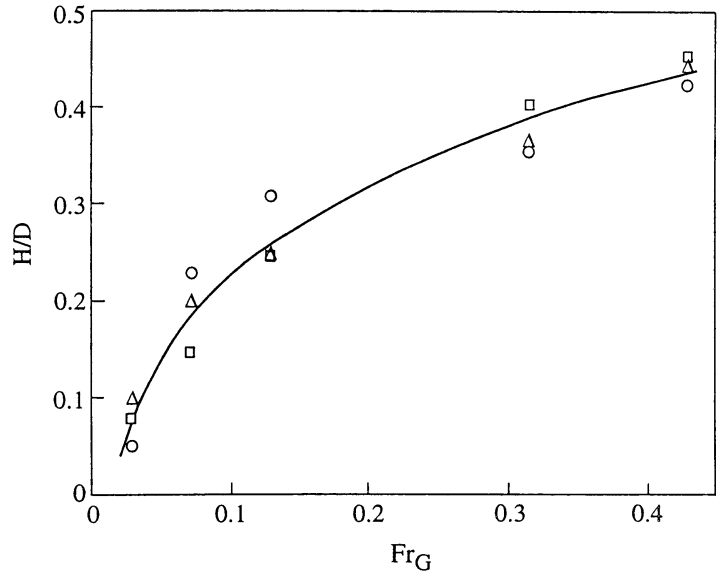

b)

Figure 7. The average bubble size: (a) non-dimensional bubble length vs. gas Froude number; (b) non-dimensional bubble height vs. gas Froude number: ○, $U_{LS} = 0.62$ m/s; □, $U_{LS} = 0.87$ m/s; △, $U_{LS} = 1.40$ m/s.

velocity at a constant water flow rate generally increases the bubble length, especially at low water velocities. In the range of superficial liquid velocities, used in the present study, the average non-dimensional bubble length L/D vs. the superficial gas velocity can be expressed by a single curve shown in figure 7(a) within standard deviation 15%. We note here that for a wider range of water flow rate, the error caused by this simplification is not acceptable and should be taken into account (Dukler and Hubbard 1975). In addition to the average values of bubble length, it has been shown by Barnea and Taitel (1993) that the standard deviation for the fully developed flow may vary from 23 to 41%.

Figure 7(b) shows the average non-dimensional bubble height H/D vs. the gas Froude number under different superficial liquid velocities, where H is the maximum bubble height, D is the pipe diameter. The bubble height was defined by visual observations of large-length bubbles which touch the upper part of the wall and are separated by water slugs. No significant influence of the non-dimensional superficial liquid velocity is observed. This confirms the results from the experiment of Nicholson *et al.* (1978) in this range of air and water flow rates. Similarly to the bubble length, for wider range of air and water flow rates the data on the bubble height are more dispersed and cannot be incorporated into one curve like that shown in figure 7(b). Each parameter, L or H, of individual bubbles is statistically independent.

The fact that the values of L/D and H/D are independent of the superficial liquid velocity indicates that under these conditions the mechanism of wave formation is independent of the liquid flow rate. Experimental and analytical studies (Dukler and Hubbard 1975) have shown that, for the range of flow conditions over which an intermittent flow is observed, a wave is formed and grows rapidly to block the flow.

In order to determine the boundaries of the stratified flow regime, the linear stability analysis proposed by Hanratty and Hershman (1961) and more recently also adopted by Andreussi *et al.* (1985) may serve as an appropriate tool. Unfortunately, this analysis is rather complicated, and the results have not been expressed using a simple equation. However, the analysis can be drastically simplified when the inertia terms in the liquid momentum equation are neglected and a finite solitary wave on a flat horizontal surface is considered. This approach has been used by Barnea and Taitel (1986). In this case, the stability criterion for channel flow is given by [3], where C depends on h and D:

$$u_G > C\left[\frac{g(\rho_L - \rho_G)h}{\rho_G}\right]^{1/2} \qquad [3]$$

where u_G is the gas velocity, h is the distance between the upper plate and the equilibrium liquid level. In a dimensionless form the criterion [3] becomes:

$$\frac{u_G}{\sqrt{gD}}/C\left[\frac{(\rho_L - \rho_G)}{\rho_G}\frac{h}{D}\right]^{1/2} > 1. \qquad [4]$$

Note that for given values of r_L and r_G, all terms in [4] are functions of $u_G/\sqrt{gD}$ and h/D only. In the range $0.90 \leq U_{LS}/\sqrt{gD} \leq 2.00$, since h/D is a function of $u_G/\sqrt{gD}$ only, the wave formation in the intermittent flow is uniquely determined by the gas velocity (when the liquid velocity is larger than a certain threshold value, see figure 5). This statement reflects the qualitative side of the phenomena. The experimental data on the flow patterns and transition boundaries are usually mapped in a two-dimensional plot. Figure 5 shows an example of such a map. Curve 1 in figure 5 represents the locus of such points; below this curve stratified flow exists. If the superficial liquid velocity is smaller than $U_{LS} = 0.1$ m/s, the wave formation does not occur in the range $U_{GS} < 1.0$ m/s.

4.1.3. *Bubble velocity and frequency*. The bubble velocity was determined for all of the bubbles which have length larger than the tube diameter D. Then, the average bubble velocity was calculated. Figure 8 shows a plot of the non-dimensional average bubble velocity vs. the gas Froude number. The experimentally determined values agree, within a standard deviation of $\pm 11\%$, with the correlation of Taitel and Barnea (1990):

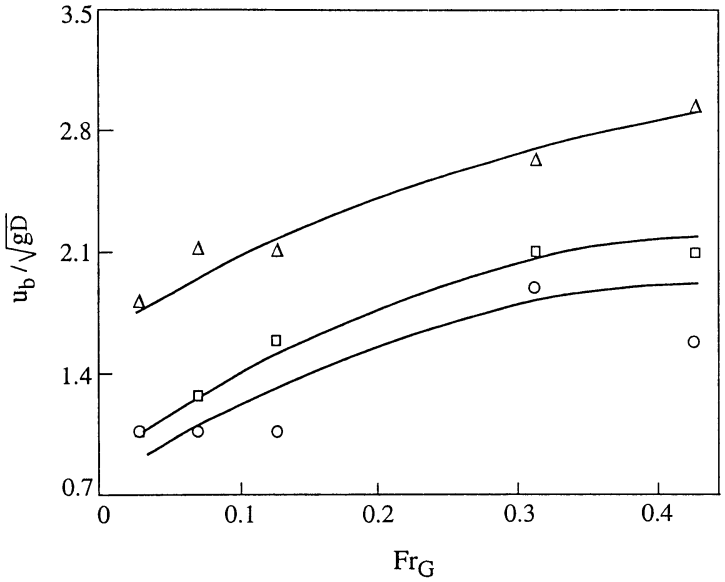

Figure 8. The measured average bubble velocity vs. the gas Froude number: ○, $U_{LS}=0.62$ m/s; □, $U_{LS}=0.87$ m/s; △, $U_{LS}=1.40$ m/s.

$$u_b = 1.2(U_{LS} + U_{GS}) \quad [5]$$

where U_{LS}, U_{GS} are superficial velocities of liquid and gas, respectively.

According to the dimensional analysis, we calculated the combination fL/u_b, where f is the frequency of the bubbles, L is the average bubble length, and u_b is the bubble velocity. The total time of fluid residence on the heated wall τ can be divided into the residence time of the bubbles ($\Delta\tau_b$) and the residence time ($\Delta\tau_s$) of the liquid slugs on the heated wall:

$$\tau = \Delta\tau_b + \Delta\tau_s. \quad [6]$$

During this period τ, there is a total of n bubbles passing over the heated wall, hence

$$f = \frac{n}{\tau} \quad [7]$$

$$\Delta\tau_b = \frac{nL}{u_b} \quad [8]$$

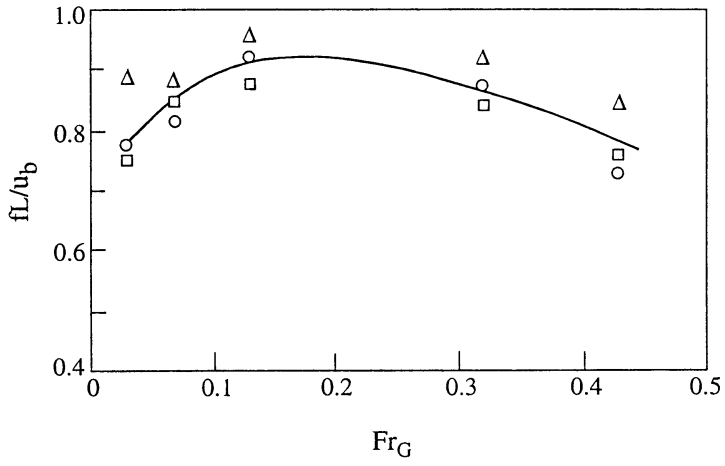

Figure 9. Parameter fL/u_b vs. the gas Froude number: ○, $U_{LS}=0.62$ m/s; □, $U_{LS}=0.87$ m/s; △, $U_{LS}=1.40$ m/s.

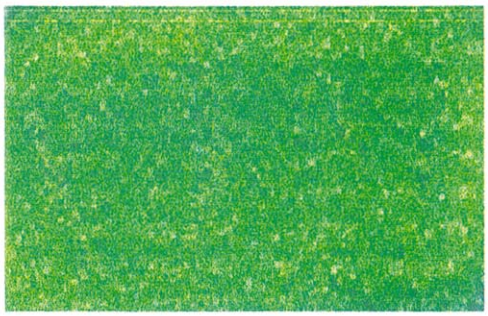

a)

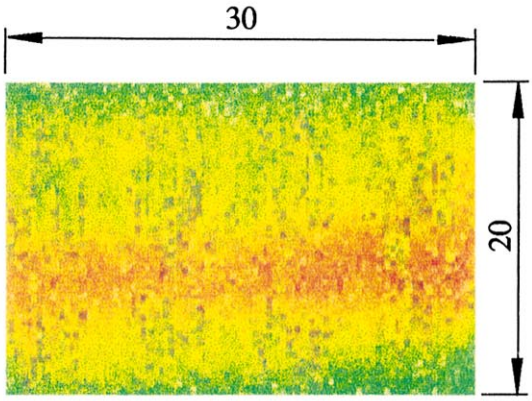

b)

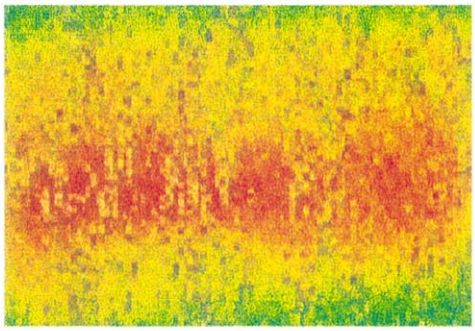

c)

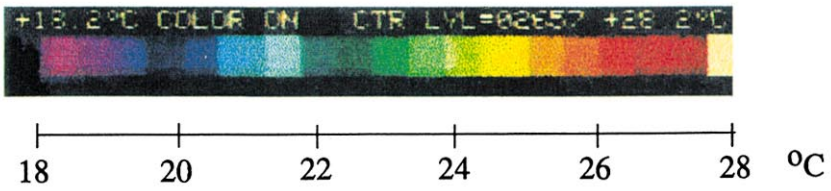

Figure 10. The temperature field on the upper part of the tube: (a) water flow; (b) air–water mixture;

Table 2. Local heat transfer coefficients

Superficial liquid velocity U_{LS} (m/s)	Superficial gas velocity U_{GS} (m/s)	Air–water flow Time-averaged local heat transfer coefficients α_θ (W/m^2 K)					
		$\theta = 0$	$\theta = 0.055$	$\theta = 0.110$	$\theta = 0.165$	$\theta = 0.220$	$\theta = 0.275$
0.62	0.02	1200	1450	1700	2900	3100	3400
	0.05	860	1100	1400	2700	3200	3400
	0.09	830	1100	1400	2800	3100	3200
	0.22	1370	1550	1700	2900	3300	3400
	0.30	1400	1600	1900	3000	3200	3300
0.87	0.02	3000	3150	3300	4200	4500	4600
	0.05	2800	3000	3200	4100	4400	4500
	0.09	2600	2800	3000	4000	4300	4500
	0.22	2700	2900	3100	4100	4400	4400
	0.30	2900	3050	3300	4200	4400	4600
1.40	0.02	6500	6650	6700	6900	6950	6950
	0.05	6400	6450	6500	6800	6950	7000
	0.09	5500	5650	5800	6600	6700	6800
	0.22	5800	5900	6000	6700	6800	6900
	0.03	6400	6450	6500	6900	6950	6950

and

$$\frac{fL}{u_b} = \frac{\Delta\tau_b}{\tau}. \qquad [9]$$

The physical meaning of this non-dimensional group of flow parameters, fL/u_b, is the portion of time occupied by the air on the heated wall. We checked the validity of this group by an analysis of the time-dependent temperature distribution on the top of the heated wall. We assume that when the wall temperature retains for some time its almost constant minimum value, a water slug passes over the measurement point ($\Delta\tau_s$). From the instant when the tem-

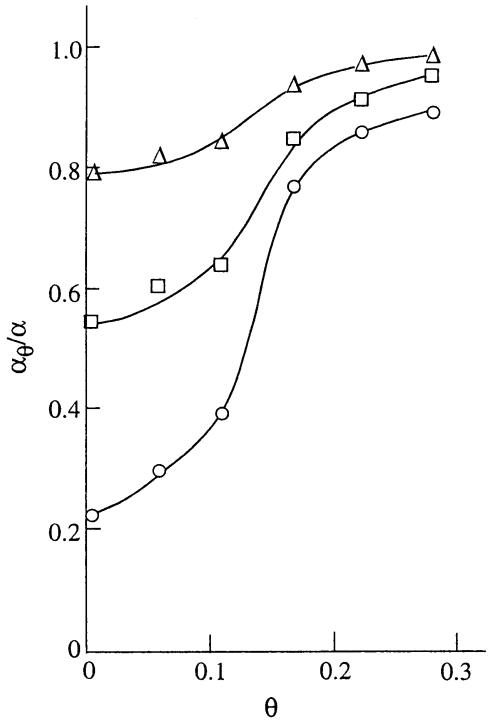

Figure 11. Variation of the circumferential heat transfer coefficient, at $U_{GS} = 0.09$ m/s: ○, $U_{LS} = 0.62$ m/s; □, $U_{LS} = 0.87$ m/s; △, $U_{LS} = 1.4$ m/s.

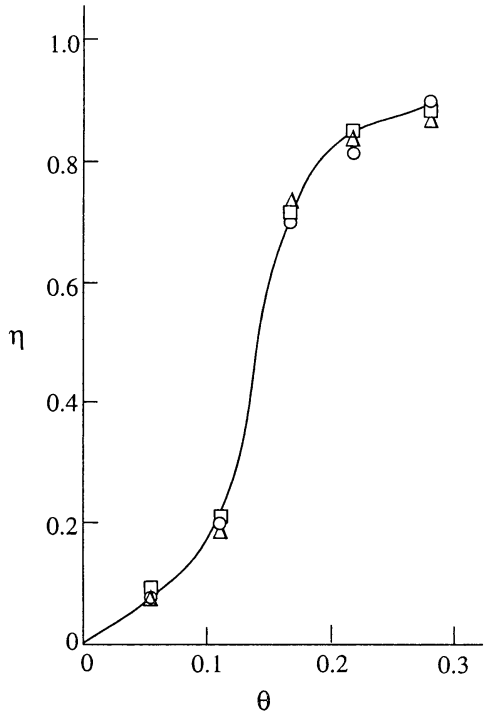

Figure 12. Variation of the circumferential parameter η, at, $U_{GS}=0.02$–0.30 m/s: ○, $U_{LS}=0.62$ m/s; □, $U_{LS}=0.87$ m/s; △, $U_{LS}=1.4$ m/s.

perature begins to increase, and till the moment it returns to the minimum value, a bubble is passing ($\Delta\tau_b$). The results are in good agreement with those obtained from video recordings.

Figure 9 shows a plot of fL/u_b vs. the gas Froude number Fr_G under various water flow rates. For the liquid Froude numbers from $Fr_L=0.90$ to 2.00, the parameter fL/u_b reaches its maximum value at about the same value of $Fr_G=0.13$.

4.2. *Heat transfer on the upper part of the tube*

Primary attention was paid to evaluation of the heat transfer coefficient and to comparison of the results with flow parameters defined for an isothermal flow. The experiments have been performed with a two-component system in which heat is transferred without change of phase, at low values of the heat flux. For each superficial gas and liquid velocity, the heat flux was chosen to keep the temperature difference between the wall and the fluid at no more than 10°C. For example, at $U_{LS}=0.62$ m/s the heat flux varied significantly from 0.7 to 3.1 kW/m^2 with the air velocity varying from 0.05 to 0.30 m/s.

4.2.1. *The instantaneous variation of circumferential wall temperature*. Figure 10(a–c) illustrates a typical temperature field on the upper part of the tube, recorded at different time instant. The superficial liquid and gas velocities were $U_{LS}=1.40$ m/s, $U_{GS}=0.30$ m/s. The heat flux is 18,600 W/m^2. The flow is from the right to the left, the colour shades are proportional to the wall temperatures. One can see that the temperature field changes with time, because the flow parameters (bubble length, velocity, and frequency) change. The picture of the dependence of the thermal pattern, which emerges from these visualization studies, on the flow is as follows. In a slug flow, when the wall is covered by liquid, the wall temperature is lower [figure 10(a)]. When the wall is covered by an air bubble, the wall temperature increases [figure 10(b)] and reaches its maximum value [figure 10(c)]. The time interval between figure 10(a) and figure 10(b) is 0.04 s; the time interval between figure 10(a) and figure 10(c) is 0.12 s.

4.2.2. *The time-averaged local heat transfer coefficients*. The intermittent flow at low gas velocities with air bubbles, slowly moving along the upper part of the pipe, and the resulting low heat transfer coefficients in this region, can be expected to yield large circumferential wall temperature differences. High circumferential non-uniformity, at high values of the heat flux, leads

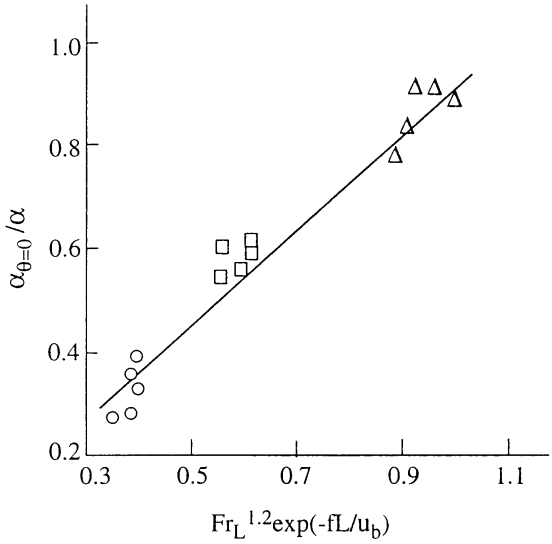

Figure 13. Effect of bubble parameters on heat transfer on top of the tube: ○, $Fr_L = 0.9$; □, $Fr_L = 1.3$; △, $Fr_L = 2.0$.

to a high thermal stress and affects both the carried load and operating life of the tube. The results are given in table 2. In figure 11, the ratio of the two-phase heat transfer coefficient to that for the single-phase liquid, α_θ/α, is plotted vs. non-dimensional angle θ from the top of the tube. Figure 11 shows that the heat transfer coefficient increases from the top of the pipe ($\theta = 0$) to its lower part and reaches about 90–95% of its maximum value when θ exceeds about 0.3. At $\theta = 0$, the non-dimensional heat transfer coefficient may decrease more than four times in comparison to that for a single-phase water flow.

In figure 11, the non-dimensional heat transfer coefficient is plotted for several values of liquid superficial velocity while the gas superficial velocity is 0.09 m/s. The effect of these parameters on α_θ/α is not uniform. We assume that a dependence of α_θ/α may be described by a single line, using the non-dimensional parameter:

$$\eta = \frac{\alpha_\theta - \alpha_{\theta=0}}{\alpha - \alpha_{\theta=0}} \qquad [10]$$

where α and α_θ are for the same liquid mass flow rate. The results are shown in figure 12.

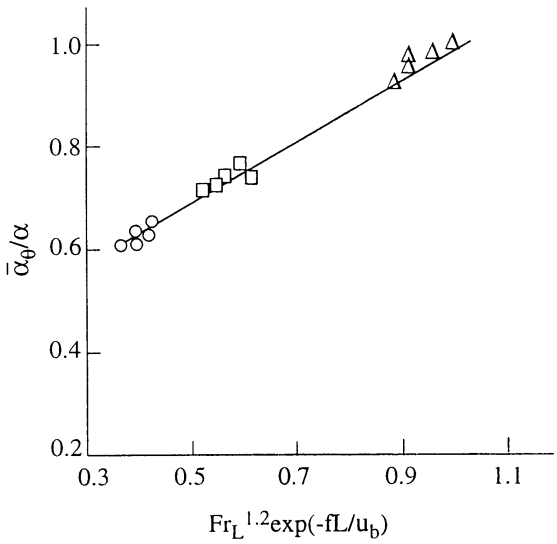

Figure 14. Effect of bubble parameters on heat transfer on the upper part of the tube, $\theta \leq 0.3$: ○, $Fr_L = 0.9$; □, $Fr_L = 1.3$; △, $Fr_L = 2.0$.

The single function η describes experimental results for all the conditions used in the present work. In particular, for $\mathrm{Fr_G} = 0.43$ when almost half of the tube is filled with gas, the value of the heat transfer coefficient at the bottom of the tube is the same as that in the clear water. This preservation of the heat transfer mechanism, regardless of the oscillation imposed in the present study, is similar to some findings of Brereton *et al.* (1990). Considering the response of the turbulent boundary layer to a free-stream unsteadiness, they support our view of the near-wall motions in the turbulent boundary layer as most stable to an external disturbance.

The curve $\eta = f(\theta)$ describes all the runs with standard deviation 10% at $\theta = 0.055$ and 0.110, and with standard deviation 5% at $\theta = 0.165$, 0.220 and 0.275.

4.3. *Effect of bubble parameters on heat transfer at the top of the tube*

Under the experimental conditions of the present study, the adiabatic flow parameters can be expected to offer a first guide to the thermal behaviour of intermittent elongated bubble flow.

It should be noted that the range of values of fL/u_b is small to establish the relationship between the heat transfer on the top of the tube and bubble parameters. We assume that if the mass flow of air approaches zero, the cross-section of the tube is full of water, and the heat transfer coefficient at the top is about the same as in the clear water. In this case, $\alpha_{\theta=0}/\alpha$ tends to unity. Thus, we decided to use an exponential form to describe this relationship:

$$\frac{\alpha_{\theta=0}}{\alpha} = 0.95\mathrm{Fr_L^{1.2}} \exp\left(-\frac{fL}{u_\mathrm{b}}\right). \tag{11}$$

This relation is shown in figure 13 and describes the experimental data in the range $0.9 < \mathrm{Fr_L} < 2.0$ and $0.03 < \mathrm{Fr_G} < 0.43$ with standard deviation 12%.

4.4. *Space-averaged heat transfer coefficient*

Now we consider the equation

$$\bar{\eta} = \frac{1}{\theta^*}\int_0^{\theta^*} \eta \, \mathrm{d}\theta \tag{12}$$

where θ^* is the ratio of the area, F_u, of the upper part of the tube, in which significant change of heat transfer coefficient takes place, to the whole tube surface area, F. The behaviour of η vs. θ (see figure 10) shows that at $\theta^* = 0.3$ the value of h reaches about 95% of its maximum. At $\theta^* = 0.3$ the calculated value is $\bar{\eta} = 0.40$. On the other hand

$$\bar{\eta} = \frac{1}{\theta^*}\int_0^{\theta^*} \frac{\alpha_\theta - \alpha_{\theta=0}}{\alpha - \alpha_{\theta=0}} \, \mathrm{d}\theta \tag{13}$$

and

$$\bar{\eta} = \frac{1}{\theta^*}\int_0^{\theta^*} \alpha_\theta \, \mathrm{d}\theta = \frac{1}{\theta^*}\int_0^{\theta^*} \alpha_{\theta=0} \, \mathrm{d}\theta - \eta\theta^*(\alpha - \alpha_{\theta=0}). \tag{14}$$

Taking into account [13] and $\bar{\eta} = 0.40$, [14] can be expressed as follows:

$$\bar{\alpha}_\theta = \alpha[0.40 + 0.54\mathrm{Fr_L^{1.2}} \exp(-fL/u_\mathrm{b})]. \tag{15}$$

The latter relation is shown in figure 14, and describes the experimental data for the averaged heat transfer coefficient on the upper part of the tube, $\theta \leq 0.3$, in the range $0.9 < \mathrm{Fr_L} < 2.0$ and $0.03 < \mathrm{Fr_G} < 0.43$ with standard deviation 6%.

It should be noted that the value of θ^* is not the same as the ratio of the upper part area F_u, on which a periodic gas–liquid flow exists, to the whole tube area F. The maximum ratio $Z = F_\mathrm{u}/F$ may be calculated from the dependence of the non-dimensional maximum bubble height on air Froude number (figure 7), and changes from $Z = 0.20$ to $Z = 0.45$. However, according to the results plotted in figures 11 and 12, the most significant change of the heat

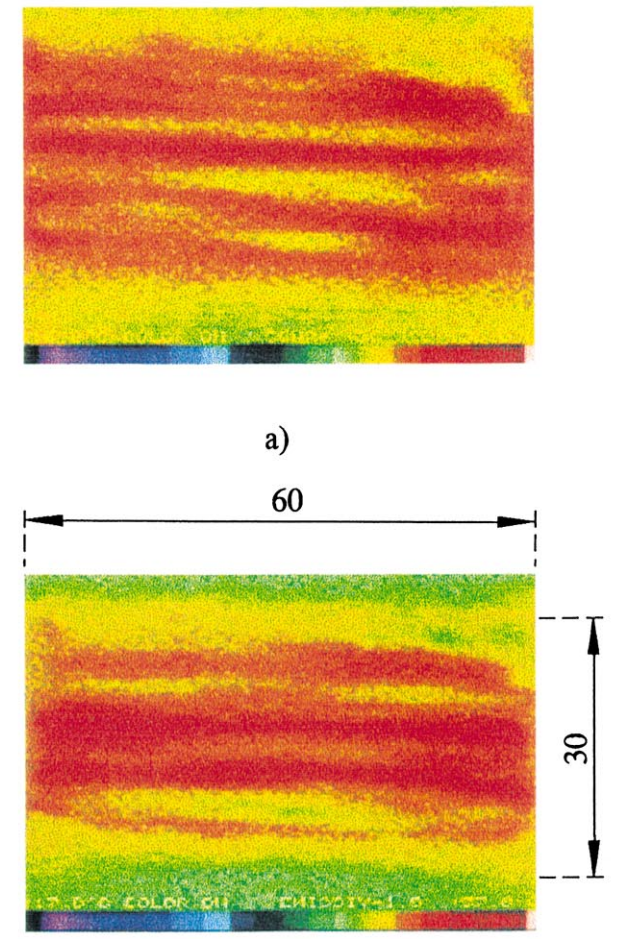

Figure 15. Thermal pattern on the heated wall at $\theta > 0.3$, $U_{LS} = 0.62$ m/s: (a) water flow; (b) $Fr_G = 0.03$; (c) $Fr_G = 0.43$ (window boundaries are given by - - -).

Table 3. Summary of heated length in heat transfer studies in horizontal air–water flow

Investigator	Pipe diameter D (m)	Type of heating	Dimensionless heated length x/D
Johnson and Abou-Sabe (1952)	0.022	steam	215
Fried (1954)	0.019	steam	248
Shoham *et al.* (1982)	0.0381	electrical	46
Kago *et al.* (1986)	0.0515	electrical	9.5
Deshpande *et al.* (1991)	0.028	electrical	61
	0.057		30

transfer coefficient occurs at $Z = \theta^*$. At the range $Z > \theta^*$ the heat transfer coefficient α may be calculated using the solution functions for the turbulent flow in a circular tube for the thermal entry length (Kays, 1966).

4.5. *Heat transfer in the liquid phase*

Consider the fact that as bubble height, length and frequency change with the gas Froude number, the heat transfer does not alter. Figure 15(a–c) illustrates no changes in the thermal pattern on the wall, when the superficial liquid velocity is 0.62 m/s and superficial gas velocity increases from 0.02 to 0.3. The IR images indicate that in this case the thermal field consists of high and low temperature streaks. It is a very interesting feature: the air occupies roughly the upper half of the tube, the waves of great amplitude appear on the liquid surface, but the heat transfer coefficient does not change.

The heat transfer depends mainly on the liquid velocity, even at gas flow rates higher than those utilized in the present study. The same conclusion was drawn by Kago *et al.* (1986). In their experiments, the water velocity range was 0.25–1.0 m/s. It was shown that in the range of the superficial gas velocity $U_{GS} = 0.2$–1.0 m/s the heat transfer coefficient was nearly independent of the gas velocity.

It is known that the effect of surface waves on a turbulent boundary layer manifests itself in a change of the mean and fluctuation velocity fields. Excitation of surface waves is accompanied by an increase in the mean velocity near a smooth wall, as well as the growth of the maximum turbulence intensity. The turbulent boundary layer thickness is also reduced considerably. However, these changes in the flow field do not affect practically the average value of the shear stress at the wall (Kemp and Simons, 1982, 1983). The effect of surface waves on bursting characteristics (the mean value of streak spacing and burst frequency) is also weak (Hetsroni *et al.* 1997).

Hetsroni *et al.* (1996) assumed that bursting plays a dominant role in the process of heat transfer through the sublayer of a turbulent boundary layer. It was shown that this assumption leads to the results which agree with numerous experimental data on heat removal from the wall at various Prandtl numbers. In accordance with the assumption of Hetsroni *et al.* (1996), we can conclude that surface waves cannot affect the average heat removal from the wall in a turbulent boundary layer.

Table 4. Comparison of the data reported by Kago *et al.* (1986) with the values calculated in the present study

Superficial liquid velocity U_{LS} (m/s)	Superficial gas velocity U_{GS} (m/s)	Overall heat transfer coefficient $\bar{\alpha}$ (W/m^2 K)	
		Kago *et al.* (1986) $D = 0.0515$ m	Present study $D = 0.0492$ m
0.25	0.2	1000	1140
	0.3	1000	1150
	0.1	2000	2050
0.5	0.2	2100	2050
	0.3	2150	2100
	0.1	3900	3750
1.0	0.2	3900	3750
	0.3	3950	3800

Assuming that in the liquid phase of gas–water flow the heat transfer coefficient is independent of gas velocity, the overall space- and time-average heat transfer coefficient for intermittent flow in a horizontal tube can be calculated as

$$\bar{\alpha} = 0.15\bar{\alpha}_\theta + 0.85\alpha. \quad [16]$$

4.6. *Interpretation of the results obtained in the thermal entrance length*

At the cross-section where the heating starts, the heat transfer coefficient has its highest value. Thermal entrance length is defined as the distance between these cross-sections and the cross-section at which the coefficient reaches its constant value. This distance depends on the character of the flow. If the experimental conditions are such that the heat transfer coefficient does not reach a constant value, an interpretation problem arises, namely, whether it is possible to apply the results to an intermittent flow with fully developed velocity and temperature profiles.

Table 3 presents the details on heated lengths from the literature. One can see that most of the experiments were performed with the relation of the heated length to the pipe diameter $x/D \geq 30$, except for the work by Kago *et al*. (1986) who used $x/D = 9.5$. The heat transfer coefficient was expressed by a dimensionless correlation including liquid hold-up (the fraction of the cross-section occupied by the liquid), liquid superficial velocity, and the properties of the liquid. This correlation fits all the data in the literature, including those of Johnson and Abou-Sabe (1952) for $x/D = 255$, and Fried (1954) for $x/D = 248$. It was shown that for the intermittent flow, an appropriate selection of the two-phase flow parameters makes it possible to express the heat transfer coefficient by a single equation for a broad range $9.5 < x/D < 248$. Hence, the data of Kago *et al*. (1986) may be considered as if obtained for a fully developed temperature profile.

The results of the present study show a considerable variation of the heat transfer coefficient along the tube both in clear water and air–water flow, see figure 3. On the other hand, a ratio of the heat transfer coefficient in air–water flow to that in clear water is independent of x/D in the range of $0.45 \leq x/D \leq 2.4$.

Let us consider now a flow with fully developed velocity and temperature profiles. The heat transfer coefficient for clear water is given by Kays (1966) as

$$\mathrm{Nu} = 0.0155\mathrm{Re}^{0.83}\mathrm{Pr}^{0.5}. \quad [17]$$

We have calculated α and α_θ from [17] and [15], respectively, and used the results to calculate the overall heat transfer coefficient $\bar{\alpha}$ from [16]. We assume, see figure 9, that fL/u_b does not depend on the superficial liquid velocity. Hence, we can compare the calculated value of $\bar{\alpha}$ with the experimental results of Kago *et al*. (1986) even when the liquid Froude numbers in their work were, in certain cases, smaller than those in our study. The comparison, presented in table 4, shows a fairly good agreement between our calculations and the experimental results of Kago *et al*. (1986).

5. CONCLUSIONS

The circumferential variation of the heat transfer coefficient in a horizontal tube has been analysed. It has been shown how the results on the heat transfer can be related to hydrodynamic phenomena accompanying the intermittent two-phase flow.

The major factors which affect the heat transfer coefficient for the upper part of the horizontal pipe are the superficial liquid velocity, and bubble length, velocity and frequency. At a low superficial liquid velocity, the heat transfer coefficient reaches its minimum value which is about four times smaller than that for the single-phase water flow with the same velocity. For the lower part of the tube, the heat transfer coefficient appears to be independent of bubble length, velocity and frequency.

The results of the present study can be used to calculate the top-to-bottom temperature difference for the heat transfer to air–water flow in a horizontal tube. These results will also serve as a reference basis for the studies on inclined and vertical tubes.

Acknowledgements—This research was supported by both the Basic Research Foundation administered by the Israeli Academy of Sciences and Humanities, by a grant from the NCRC and the Forschungszentrum Jülich GMBH (KFA), and by the Fund of Promotion of Research at the Technion. Baigeng Hu was supported by a Lady Davis Postdoctoral Fellowship. Jinghai Yi was supported by an Israel Higher Education Council Postdoctoral Fellowship. A. Mosyak was partially supported by the Center for Absorption in Sciences, Ministry of Immigrant Absorption (State of Israel).

REFERENCES

Andreussi, P., Asall, J. C. and Hanratty, T. J. (1985) Initiation of roll waves in gas–liquid flow. *AIChE J.* **31,** 119–126.

Andritsos, N. and Hanratty, T. J. (1987) Interfacial instabilities for horizontal gas–liquid flows pipelines. *Int. J. Multiphase Flow* **13,** 583–603.

Barnea, D. and Taitel, Y. (1986) Flow pattern transitions in two-phase gas–liquid flows. *Encyclopedia of Fluid Mechanics*, ed. N. Cheremisinoff, Vol. 3. Gulf Publishing Company, pp. 403–474.

Barnea, D. and Taitel, Y. (1993) A model for slug length distribution in a gas–liquid slug flow. *Int. J. Multiphase Flow* **19,** 829–838.

Brereton, G. J., Reynolds, W. S. and Jayaraman, R. (1990) Response of a turbulent boundary layer to sinusoidal free-stream unsteadiness. *J. Fluid Mech.* **221,** 131–159.

Deshpande, S. D., Bishop, A. A. and Karandikar, M. (1991) Heat transfer to air–water plug–slug flow in horizontal pipes. *Ind. Eng. Chem. Fundam.* **30,** 2172–2180.

Dukler, A. E. and Hubbard, E. G. (1975) A model for gas–liquid slug flow in horizontal and near horizontal tubes. *Ind. Eng. Chem. Fundam.* **14,** 337–347.

Foukano, T. and Ousaka, A. (1989) Prediction of the circumferential distribution of film thickness in horizontal and near horizontal gas–liquid annular flows. *Int. J. Multiphase Flow* **15,** 403–419.

Fried, L. (1954) Pressure drop and heat transfer for two-phase two-component flow. *AIChE Symp. Ser.* **50** (9), 47–51.

Hand, N. P. and Spedding, P. L. (1993) Horizontal gas–liquid flow at close to atmospheric conditions. *Chem. Eng. Sci.* **48,** 2283–2305.

Hanratty, T. J. and Hershman, A. (1961) Initiation of roll waves. *AIChE J.* **7,** 488–497.

Hetsroni, G. and Rozenblit, R. (1994) Heat transfer to a liquid–solid mixture in a flume. *Int. J. Multiphase Flow* **20,** 671–689.

Hetsroni, G., Yarin, L. P. and Kaftori, D. (1996) A mechanistic model for heat transfer from a wall to fluid. *Int. J. Heat Mass Transfer* **39,** 1475–1478.

Hetsroni, G., Mosyak, A. and Yarin, L. P. (1997) Effect of surface waves on heat transfer in natural and forced convection. *Int. J. Heat Mass Transfer* **40,** 2219–2229.

Hughmark, G. A. (1965) Hold-up and heat transfer in horizontal slug gas–liquid flow. *Chem. Eng. Sci.* **20,** 1007–1010.

Jepson, W. P. and Taylor, R. E. (1993) Slug flow and its transitions in large-diameter horizontal pipes. *Int. J. Multiphase Flow* **19,** 411–420.

Johnson, H. A. and Abou-Sabe, A. H. (1952) Heat transfer and pressure drop for turbulent flow of air–water mixtures in a horizontal pipe. *Trans. ASME*, 977–987.

Kago, T., Saruwatari, T., Kashima, M., Morooka, S. and Kato, Y. (1986) Heat transfer in horizontal plug and slug flow for gas–liquid and gas–slurry systems. *J. Chem. Eng. Jpn* **19,** 125–131.

Kays, W. M. (1966) *Convective Heat and Mass Transfer*. McGraw-Hill, New York.

Kemp, P. H. and Simons, R. R. (1982) The interaction between waves and a turbulent current: waves propagating with the current. *J. Fluid Mech.* **116,** 227–250.

Kemp, P. H. and Simons, R. R. (1983) The interaction of waves and a turbulent current: waves propagating against the current. *J. Fluid Mech.* **130,** 73–89.

Kokal, S. L. and Stanislav, J. F. (1989) An experimental study of two-phase flow in slightly inclined pipes—I. Flow patterns, II. Liquid hold-up and pressure drop. *Chem. Eng. Sci.* **44,** 665–693.

Lin, P. Y. and Hanratty, T. J. (1986) Prediction of the initiation of slugs with linear stability analysis. *Int. J. Multiphase Flow* **12,** 79–98.

Lin, P. Y. and Hanratty, T. J. (1987) The effect of pipe diameter on flow patterns for air–water flow in horizontal pipes. *Int. J. Multiphase Flow* **13,** 549–563.

Mandhane, J. M., Gregory, G. A. and Aziz, K. (1974) Flow pattern map for gas–liquid flow in horizontal pipes. *Int. J. Multiphase Flow* **1,** 537–553.

Mehta, D. C. (1984) Full-scale cold-flow modelling of the SRC-I slurry heater at Create Inc. DOE Report No. DOE/OR/03054-58 (DE84013792).

Moalem Maron, D., Yacoub, N., Brauner, N. and Naot, D. (1991) Hydrodynamic mechanisms in the horizontal slug pattern. *Int. J. Multiphase Flow* **17,** 227–245.

Nicholson, M. K., Aziz, K. and Gregory, G. A. (1978) Intermittent two-phase flow in horizontal pipes: predictive models. *Can. J. Chem. Eng.* **56,** 653–663.

Paras, S. V. and Karabellas, A. J. (1991) Droplet entertainment and deposition in horizontal annular flow. *Int. J. Multiphase Flow* **17,** 455–468.

Ruder, Z., Hanratty, P. J. and Hanratty, T. J. (1989) Necessary conditions for the existence of stable slugs. *Int. J. Multiphase Flow* **15,** 209–226.

Shoham, O., Dukler, A. E. and Taitel, Y. (1982) Heat transfer during intermittent/slug flow in horizontal tubes. *Ind. Eng. Chem. Fundam.* **21,** 312–318.

Spedding, P. L. and Spence, D. R. (1993) Flow regimes in two-phase gas–liquid flows. *Int. J. Multiphase Flow* **19,** 245–280.

Sun, G., Wadekar, V. V. and Hewitt, G. F. (1994) Heat transfer in horizontal slug flow. *Proceedings of the 10th International Heat Transfer Conference*, Brighton, pp. 271–276.

Taitel, Y. and Barnea, D. (1990a) Two-phase slug flow. *Adv. Heat Transfer* **20,** 83–132.

Taitel, Y. and Dukler, A. E. (1976) A model for predicting flow regime transitions in horizontal and near horizontal gas–liquid flows. *AIChE J.* **22,** 47–55.

Wallis, G. B. (1968) Phenomena of liquid transfer in two-phase dispersed annular flow. *Int. J. Heat Mass Transfer* **11,** 783–785.

Whalley, P. B. and Hewitt, G. F. (1978) The correlation of liquid entrainment fraction and entrainment rate in annular two-phase flow. UKAEA, Harwell, AERE-Report 9187.

Woods, B. D. and Hanratty, T. J. (1996) Relation of slug stability to shedding rate. *Int. J. Multiphase Flow* **22,** 809–828.